Spatiotemporal carrier dynamics in quantum wells under surface acoustic waves

A. García-Cristóbal* and A. Cantarero
Materials Science Institute, University of Valencia, P.O. Box 22085, E-46071 Valencia, Spain

F. Alsina and P. V. Santos
Paul-Drude-Institut für Festkörperelektronik, Hausvogteitplatz 5-7, 10117 Berlin, Germany
(Received 7 November 2003; published 3 May 2004)

We present a theoretical study of transport and recombination of electrons and holes in quantum wells under the piezoelectric field induced by a surface acoustic wave (SAW). Our model calculations, which include free carriers and excitons in the framework of the drift-diffusion equations, describe the spatial and time dependences of the photoluminescence intensity on excitation density and SAW amplitude, and show overall agreement with recent microphotoluminescence experiments performed on GaAs/(Al,Ga)As quantum wells and quantum wires.

DOI: 10.1103/PhysRevB.69.205301 PACS number(s): 73.63.−b, 72.20.Jv, 78.67.−n

I. INTRODUCTION

The various effects of a homogeneous (either stationary or alternating) electric field on the transport properties of semiconductors and semiconductor heterostructures have been widely investigated.[1] The influence of such a field on the optical properties is also well documented in the literature and has even provided the operating principle of optoelectronic devices such as optical modulators based on the quantum-confined Stark effect.[2] In contrast, only marginal attention has been paid so far to the interaction of an inhomogeneous and nonstationary electric field with photogenerated carriers and the subsequent effects on the optical properties. One of the easiest realizations for such a situation is provided by a surface acoustic wave (SAW) propagating in a piezoelectric semiconductor. The strain and piezoelectric fields accompanying the SAW produce a modulation of the band-edge profile of the semiconductor that moves with the SAW propagation velocity.

To our knowledge, the first observation of the influence of a SAW on the optical properties was the quenching of the excitonic photoluminescence (PL) intensity.[3–5] This effect, which has been further reported for various types of quantum wells (QW's),[6–9] has been generally ascribed to the dynamic spatial separation of the photogenerated electron-hole pairs by the SAW piezoelectric field and the subsequent reduction of the radiative recombination rate and PL intensity, much the same as happens under applied stationary (dc) fields. Nevertheless, the traveling character of the piezoelectric field associated with the SAW provides many more possibilities as compared to the dc field case, since the moving modulation can carry with it the separated electrons and holes, leading to an acoustically driven carrier transport. This has been indeed confirmed by performing spatially resolved PL measurements, which show an appreciable PL intensity at remote points along the SAW path.[3,8–12] More refined experiments have even shown the possibility of achieving spin transport and spin lifetime enhancement by the traveling SAW.[13] The acoustically induced separation and transport of the carriers has also been demonstrated to lead to strong nonlinear effects in the SAW attenuation coefficient (nonlinear acoustoelectric effect).[14,15] Nevertheless, the prospects of transporting electronic or spin excitations for long distances in QW structures are somewhat hindered by carrier diffusion parallel to the SAW wave front.[10] In an attempt to counteract this undesired effect, it has been proposed to restrict the lateral motion of the carriers by performing the SAW-induced transport along a quantum wire (QWR). Preliminary investigations show indeed an increase in the transport efficiency over that in QW systems.[16,17] A more recent proposal takes advantage of the interference of two orthogonal SAW beams to generate dynamic potential dots, where the lateral diffusion of the photogenerated carriers is largely suppressed.[18]

Despite the increasing activity in the experimental investigation of the various aspects of the SAW-induced transport, the theoretical understanding of the interplay between the SAW and the photogenerated carriers is at present very elementary. It is the purpose of this paper to introduce a theoretical model to investigate the spatiotemporal dynamics of photogenerated electron-hole pairs (and excitons) confined in a QW under a SAW propagating in the well plane. The ultimate goal will be to infer from this nontrivial dynamics the associated recombination kinetics, and the space and time dependences of the PL intensity under various experimental conditions. The model includes the interaction between free carriers, excitons, and the SAW field. In order to reduce the complexity, some simplifications have been made in the model. We have not included the SAW strain field, since its influence on the carrier transport is negligible. Its effect reduces to a weak modulation of the PL emission energy, which has been detected in energy-resolved experiments.[9,19] Furthermore, for the sake of computational simplicity we have considered a one-dimensional (along the SAW propagation direction) model for the transport. The results will thus be qualitatively valid for SAW-induced transport in QW's, but will apply directly to the case of transport in QWR systems.

The paper is organized as follows. In Sec. II, the theoretical model is described in detail. The numerical simulations are presented in Sec. III. In Sec. III A, we study a simplified version of the model in order to clarify the factors which govern the possible types of acoustically induced transport.

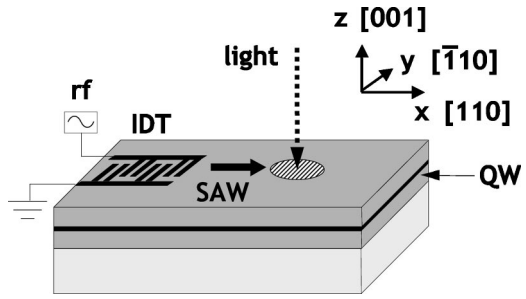

FIG. 1. Schematic illustration of the system investigated. The SAW is excited in a piezoelectric material [e.g., a (Al,Ga)As layered structure on GaAs] by applying a radio-frequency (rf) voltage to a set of interdigital transducers (IDT's). Beneath the surface, there is a quantum well [e.g., GaAs/(Al,Ga)As] where carriers are generated by the absorption of light focused on a micrometric spot. It is assumed that the PL induced by carrier recombination can be spatially resolved at any position along the SAW path.

In Sec. III B, we show numerical simulations of the spatially resolved (local or remote) PL, paying special attention to the influence of the SAW amplitude and the illumination intensity. The impact of potential fluctuations on the SAW-induced transport is examined in Sec. III C. Finally, Sec. IV summarizes the main conclusions of the work.

II. DESCRIPTION OF THE MODEL

In this section, we describe the theoretical model proposed for the spatiotemporal dynamics of the photocreated carrier concentrations and the luminescence intensity in a QW under the piezoelectric potential of a SAW traveling parallel to the well (see Fig. 1 for a schematic description of the system geometry).

Whereas impurities can substantially affect the recombination kinetics, in the good-quality, intrinsic materials of interest here their role can be disregarded in a first approximation. In order to further simplify the problem, we will restrict ourselves to sufficiently low temperatures (<20 K) so that the thermally induced generation rates can be neglected. Under the above conditions, the only carriers present in the system will be those generated by the absorption of light. In addition, we will assume that the energy relaxation of carriers is more rapid than any of the other time scales relevant to the problem, and, therefore, that the carriers are thermalized on the extrema of the lowest QW subbands. This assumption allows us to focus only on the spatial distribution of the carriers.

Under the conditions assumed above, not only electrons and holes, but also excitons formed out of them, must be considered. On account of this, two radiative recombination channels are possible: band-to-band and excitonic recombination.[20] In the following, we will first present the equations that govern the photogenerated electron and hole dynamics and the corresponding band-to-band recombination. Afterwards, we will examine how those results couple with the exciton population and excitonic recombination kinetics. At the end of this section, some hints concerning the numerical solution of the system of equations will be given.

A. Electron and hole dynamics

The simplest framework to treat the stated problem is to assume that the dynamics of electrons and holes is governed by the drift-diffusion equations coupled with the Poisson equation, which gives the internal field induced by the space charge.[21] Moreover, we will assume that the carriers are constrained to move in the plane of the QW (see Fig. 1). The propagation direction of the acoustic wave will be taken as the x axis. Only the longitudinal component (along the x axis) of the associated piezoelectric field will be considered in the present analysis.[22] In order to further simplify the problem, we will assume that the generation rate is uniform in the y direction so that the problem will effectively become one-dimensional. The inclusion of a more realistic laterally inhomogeneous generation rate would require the consideration of the spatial dynamics in the direction transverse to the SAW propagation (the y direction), thus complicating the numerical simulations. Nevertheless, since this transverse dynamics is determined only by diffusion processes, we have preferred to neglect it and focus on the longitudinal dynamics directly governed by the SAW piezoelectric field. Therefore, the electron and hole concentrations $n(x,t)$ and $p(x,t)$, respectively, obey the following one-dimensional drift-diffusion equations:[21]

$$\frac{\partial n}{\partial t}+\frac{\partial (v_n n)}{\partial x}=D_n\frac{\partial^2 n}{\partial x^2}+G-R, \tag{1a}$$

$$\frac{\partial p}{\partial t}+\frac{\partial (v_p p)}{\partial x}=D_p\frac{\partial^2 p}{\partial x^2}+G-R, \tag{1b}$$

where $G(x,t)$ and $R(x,t)$ are the electron-hole pair generation and annihilation rates (to be specified below). Within the usual classical transport theory, the drift velocities $v_n(x,t)$ and $v_p(x,t)$ depend on the electric field $E(x,t)$ through the simple relationships: $v_n=-\mu_n E$ and $v_p=+\mu_p E$, where μ_n and μ_p are the electron and hole mobilities, which are related to the corresponding diffusivities D_n and D_p by the Einstein relation.[21]

There are two contributions to the electric field E, which is expressed as $E=E_{\mathrm{SAW}}+E_{\mathrm{ind}}$. E_{SAW} is the longitudinal part of the SAW piezoelectric field,

$$E_{\mathrm{SAW}}(x,t)=E_0\cos\left[2\pi\left(\frac{x}{\lambda_{\mathrm{SAW}}}-\frac{t}{T_{\mathrm{SAW}}}+\phi\right)\right], \tag{2}$$

where E_0 denotes the amplitude of the oscillating field, and λ_{SAW} and T_{SAW} the SAW wavelength and period, respectively. The frequency and velocity of the SAW are $f_{\mathrm{SAW}}=1/T_{\mathrm{SAW}}$ and $v_{\mathrm{SAW}}=\lambda_{\mathrm{SAW}}/T_{\mathrm{SAW}}$, respectively. The phase ϕ is introduced to control the synchronization of the SAW with the switching on of the light beam responsible for carrier generation. The piezoelectric potential associated with the SAW is given by $\Phi_{\mathrm{SAW}}(x,t)=-\int dx\, E_{\mathrm{SAW}}(x,t)$ and its amplitude by $\Phi_0=(\lambda_{\mathrm{SAW}}/2\pi)E_0$. The second contribution E_{ind} is the field induced by the spatial unbalance of the electron and hole concentrations through the Poisson's equation:

$$\frac{\partial E_{\text{ind}}}{\partial x} = \frac{e(p-n)}{\varepsilon}, \tag{3}$$

where e (>0) is the magnitude of the electron charge and ε the background dielectric constant.

The rate of electron-hole pair generation in the QW mimics the nominal characteristics of the laser light impinging on the surface of the sample, and can be expressed as $G(x,t) = G_0\, g_s(x)\, f(t)$, where G_0 is the maximum generation rate, $g_s(x)$ is the spatial profile of the illumination spot, and $f(t)$ is a normalized temporal pulse shape. For definiteness, we will take for $g_s(x)$ a normalized Gaussian profile centered at x_s with full width at half maximum Δ_s. In the case of continuous wave (cw) excitation that will be considered in this paper, $f(t)$ is to be understood as a step function equal to 0 for $t<0$ and 1 for $t \geqslant 0$.

The rate of electron-hole pair annihilation rate $R(x,t)$ has two contributions: one is due to the radiative recombination accompanied with the emission of a band-gap photon and the other is associated with the capture of an electron by a hole to form an exciton in the ground state. Both processes can be modeled as a bimolecular annihilation rate, so that we can write $R(x,t) = (r+c)\, n(x,t)\, p(x,t)$, where r and c are the free-carrier radiative recombination and exciton formation coefficients, respectively. Usually, exciton formation is an extremely fast process as compared to band-to-band recombination, and, therefore, $c \gg r$. Typical values in a GaAs/(Al,Ga)As QW are $c \sim 0.1$–$10\ \text{cm}^2/\text{s}$ and $r \sim 10^{-3}$–$10^{-4}\ \text{cm}^2/\text{s}$.[20,23] Associated with the band-to-band recombination, there will be emission of band-gap photons with a rate given by $i_{\text{PL}}(x,t) = r\, n(x,t)\, p(x,t)$.

B. Exciton dynamics

The spatiotemporal dynamics of the exciton concentration $N(x,t)$ can now be written as

$$\frac{\partial N}{\partial t} = D_X \frac{\partial^2 N}{\partial x^2} + c\, np - \frac{N}{\tau_X}, \tag{4}$$

where D_X is the exciton diffusion constant and τ_X is the exciton lifetime for radiative recombination. The complementary process to exciton formation, namely the thermally induced dissociation of an exciton into free electrons and holes, will be neglected in the present study, since we are assuming sufficiently low temperatures. Since the excitons are neutral particles, the drift term does not appear in Eq. (4). As they are polarizable entities, they could drift in an inhomogeneous electric field, but this second-order effect is outside the scope of our model. Associated with the excitonic recombination, there will be emission of photons at the exciton energy with a rate given by $I_{\text{PL}}(x,t) = N(x,t)/\tau_X$.

Since our system is subjected to an electric field, most of the parameters introduced so far (i.e., μ, r, c, τ_X, . . .) depend in principle on the field E. Nevertheless, for the sake of simplicity, we consider this dependence to be weak in the field regime studied here and neglect it in our simulations. However, in the presence of an electric field, there is an additional process that must be taken into account, namely the field-induced exciton ionization to form free electron-hole pairs. This process can be incorporated in our model by introducing a new term $-N/\tau_{\text{ion}}(E)$ into Eq. (4). Here, $\tau_{\text{ion}}(E)$ is the tunneling ionization lifetime, which for the two-dimensional exciton model is given by[24]

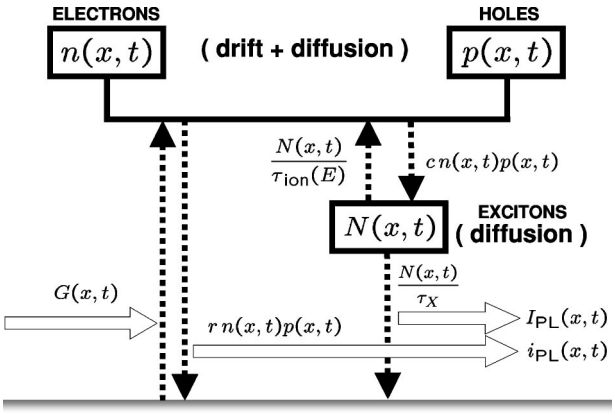

FIG. 2. Schematic representation of the theoretical model showing the various coupling mechanisms considered. All quantities are defined in the text.

$$\frac{1}{\tau_{\text{ion}}(E)} = \frac{\mathcal{E}_{2\text{D}}}{\hbar}\frac{8}{\sqrt{2\pi}}\sqrt{\frac{E_{\text{ion}}}{|E|}}\exp\left[-\frac{4}{3}\frac{E_{\text{ion}}}{|E|}\right], \tag{5}$$

where $E_{\text{ion}} = \mathcal{E}_{2\text{D}}/e a_{2\text{D}}$. Here, $\mathcal{E}_{2\text{D}}$ and $a_{2\text{D}}$ are the two-dimensional exciton binding energy and lateral extension, respectively. Although Eq. (5) was obtained assuming a uniform field, it is also meaningful for spatially dependent electric fields, as long as this variation is smooth on the scale of $a_{2\text{D}}$. The ionization of an exciton leads to the formation of an electron-hole pair, so we must supplement the generation rate G in Eq. (1) with the term $+N/\tau_{\text{ion}}(E)$.

C. Numerical details

In order to fully describe the spatiotemporal carrier dynamics, we have to solve the system of coupled nonlinear differential equations given by Eqs. (1), (3), and (4). The interrelationship between these equations is sketched in Fig. 2. The solution is given in terms of the concentrations $n(x,t)$, $p(x,t)$, and $N(x,t)$. As a by product, one can obtain the photon emission rates $i_{\text{PL}}(x,t)$ and $I_{\text{PL}}(x,t)$ (hereafter referred to as PL intensities). Since there is no possibility to obtain an analytical solution to the problem, one must resort to numerical procedures. We have chosen to discretize the equations by taking finite differences in space and time and to solve them time step after time step by using the semi-Lagrangian approach described in detail in Ref. 25. The whole procedure is designed to preserve the charge conservation inherent to the drift-diffusion equations.

III. NUMERICAL RESULTS

In this section, we will present the results of numerical simulations to illustrate the dependence of the carrier dynamics on the various parameters of the model. Since not all the

TABLE I. Parameters used in the simulations (see the text for the exact meaning of the symbols).

SAW wavelength	λ_{SAW}	5.6 μm
SAW frequency	f_{SAW}	533 MHz
Dielectric constant	ε	$11.15\varepsilon_0$
Spot width	Δ_s	2 μm
Recombination coefficient	r	10^{-3} cm^2/s
Capture coefficient	c	10 cm^2/s
Exciton radiative lifetime	τ_X	0.5 ns
Exciton binding energy	$\mathcal{E}_{2D}$	10 meV
Exciton lateral extension	a_{2D}	10 nm

parameters are equally relevant or can be varied at will in a given experiment, for definiteness we will fix some of them to their typical values in the experiments performed so far (see Table I). In particular, the SAW parameters chosen correspond to the experimental results from Refs. 8–10, in which a SAW propagates along the [110] direction on the (001) surface of a (Al,Ga)As layered structure (see Fig. 1). We will assume a SAW wavelength $\lambda_{SAW}=5.6$ μm (corresponding to a frequency of typically 510–540 MHz at 14 K in samples containing QW's). The spot width Δ_s will be kept to a value of 2 μm, which is smaller than $\lambda_{SAW}/2$. The exact values of the material parameters r, c, and τ_X were not found to be critical for the phenomena investigated, and, therefore, we take typical values for III-V QW's of moderate quality. For the calculation of the tunneling ionization lifetime, we employed values for $\mathcal{E}_{2D}$ and a_{2D} typical of a GaAs/(Al,Ga)As QW.[26]

A. Simplified conditions for the SAW-induced transport

Before showing results for the general model presented in Sec. II, it is instructive to study a simplified form of the equations in order to clarify under which conditions the SAW can induce the transport of charge and what are the essential characteristics of this transport. We will disregard for the moment the generation-recombination and the exciton formation processes as well as the space-charge-induced field. Under these conditions, both drift-diffusion equations (1) for electrons and holes are decoupled and adopt the same form, so that we need to investigate only one of them. For example, the transport equation for holes can be written as

$$\frac{\partial p(\tilde{x},\tilde{t})}{\partial \tilde{t}}+\tilde{v}\frac{\partial}{\partial \tilde{x}}[u(\tilde{x},\tilde{t})p(\tilde{x},\tilde{t})]=\tilde{d}\frac{\partial^2 p(\tilde{x},\tilde{t})}{\partial \tilde{x}^2}, \qquad (6)$$

where $u(\tilde{x},\tilde{t})=\cos[2\pi(\tilde{x}-\tilde{t}+\phi)]$ and the normalized position and time are defined as $\tilde{x}=x/\lambda_{SAW}$ and $\tilde{t}=t/T_{SAW}$, respectively. This simplified model is governed by two dimensionless parameters, namely $\tilde{v}=\mu_p E_0/v_{SAW}$, i.e., the ratio between the maximum carrier velocity in the SAW field and the SAW velocity, and $\tilde{d}=D_p/(\lambda_{SAW}v_{SAW})$, which is a measure of the diffusion length $\sqrt{D_p T_{SAW}}$ relative to the SAW wavelength λ_{SAW}. It is not our intent here to systematically investigate Eq. (6) for all possible values of $\tilde{v}$ and $\tilde{d}$. Instead, we will restrict these parameters to the range of values attainable in a typical experiment and investigate the possible transport regimes that can take place.

For the calculations, we will assume a value for the mobility of $\mu_p=1000$ cm^2/V s. The parameter $\tilde{v}$ can be independently controlled by the amplitude of the SAW field. As it will become clear below, the interesting range of $\tilde{v}$ concerning the SAW-induced transport is $\tilde{v}\sim 1$. Regarding the parameter $\tilde{d}$, the assumed mobility results in a diffusivity $D_p \simeq 1.2$ cm^2/s at a temperature of 14 K, which, for the SAW parameters reported in Table I, leads to $\tilde{d}=0.0072$. Since $\tilde{d} \ll 1$, we expect that the effects of drift under the SAW will be dominant over those of diffusion. In particular, we will investigate the following three situations: $\tilde{v}=0.5$ (corresponding to $E_0=0.149$ kV/cm), $\tilde{v}=1$ ($E_0=0.298$ kV/cm), and $\tilde{v}=1.5$ ($E_0=0.447$ kV/cm). In Fig. 3, we show the time evolution of a Gaussian concentration of width $\Delta_s=2$ μm initially centered at $\tilde{x}=1$, for these three cases. The phase of the velocity field is chosen to be $\phi=-\frac{3}{4}$, so that the maximum concentration at $\tilde{x}=1$ and $\tilde{t}=0$ coincides with a point of zero velocity and negative spatial derivative. For this choice, there is a narrowing of the initial Gaussian distribution at early times, since the negative gradient of the velocity pushes the carriers toward the node of the velocity field. Nevertheless, as time passes by and the wave moves on, a clear difference is observed in the transport regime depending on the value of $\tilde{v}$. In the following, we examine separately the results obtained for the three aforementioned values of $\tilde{v}$.

For *low fields* [see Fig. 3(a), $\tilde{v}=0.5$], the carriers initially tend to follow the SAW but, since their velocity $\mu_p E_{SAW}(x,t)$ is always lower than v_{SAW}, they experience a progressive delay with respect to it. When the phase lag of the carriers reaches the half period of negative velocity [this occurs when the carriers cross the dashed line in the upper panel of Fig. 3(a)], their distribution widens and they are forced to fall back to the velocity node of the preceding period [solid straight line in Fig. 3(a)]. This process repeats indefinitely. The global effect is that the carriers, unable to follow the wave, oscillate back and forth with the period of the SAW. Except for a slight shift of the average concentration toward the direction of propagation of the wave, there is no net SAW-induced transport.

In Fig. 3(b) we illustrate the case $\tilde{v}=1$. Since within most of the region initially occupied by the carriers their velocity is smaller than that of the SAW, they are again delayed till the point where both velocities match. For $\tilde{v}=1$ this point corresponds to the maximum of the velocity field. The carriers concentrated on that point propagate with the SAW velocity. However, due to the finite width of the distribution and the finite value of the diffusivity, some of the carriers unavoidably fall behind the maximum into the region where $\mu_p E_{SAW}(x,t)<v_{SAW}$ ($u<1$ and $\partial u/\partial \tilde{x}>0$). As in Fig. 3(a), these carriers flow back to the velocity node of the preceding period, where the process repeats again. In the overall picture, though the carriers move with the SAW velocity, there

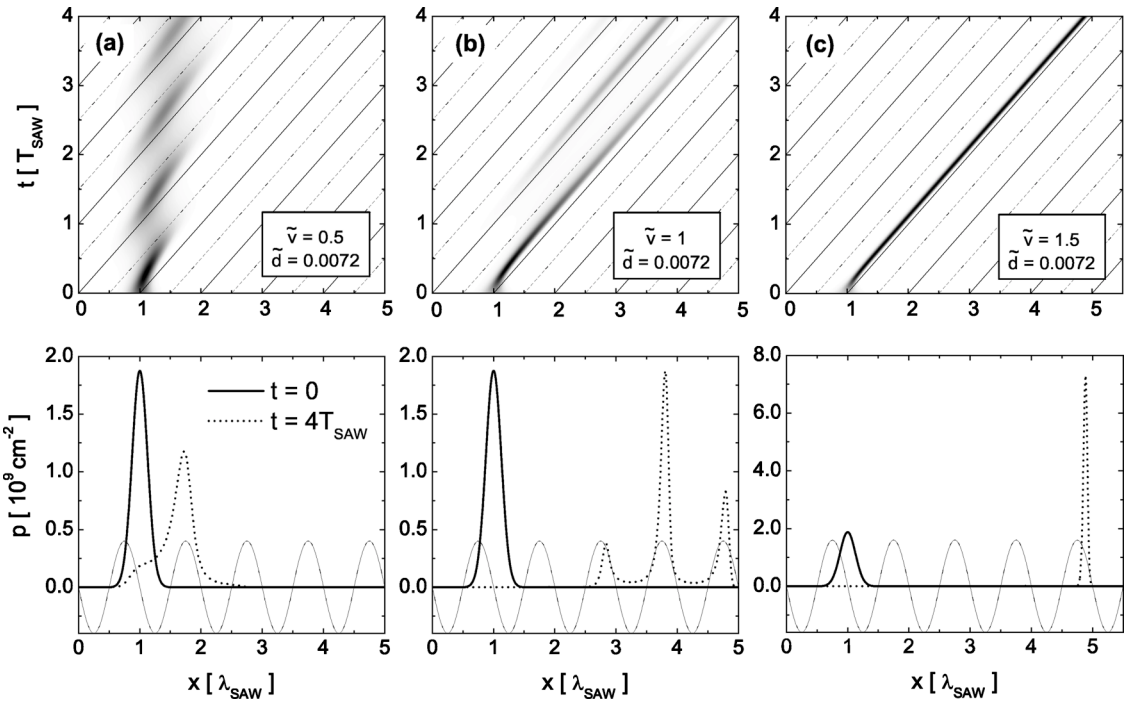

FIG. 3. Concentration $p(x,t)$ as calculated from Eq. (6) with normalized velocities: (a) $\tilde{v}=0.5$, (b) $\tilde{v}=1$, and (c) $\tilde{v}=1.5$. For all three cases, the normalized diffusivity is $\tilde{d}=0.0072$. The upper panel in each figure shows a gray scale plot of p in the (x,t) plane. The gray scale is linear between 0 (white areas) and (a) $p_{\max}=2.8\times10^9$ cm^{-2}, (b) $p_{\max}=4.9\times10^9$ cm^{-2}, and (c) $p_{\max}=7.3\times10^9$ cm^{-2} (black areas). The straight lines indicate the points where the velocity u is zero and its spatial derivative $\partial u/\partial\tilde{x}$ is negative (solid lines) or positive (dashed lines). The lower panel in each figure shows $p(x,t)$ at times $t=0$ (heavy line) and $t=4T_{\mathrm{SAW}}$ (dotted line), together with the corresponding value of $u(\tilde{x},0)$ (solid line, rescaled to fit in the graph).

is at the same time a continuous redistribution among the different periods of the wave, which eventually limits the maximum transport distance.

Finally, in the *high-field regime* [Fig. 3(c), $\tilde{v}=1.5$], the carriers concentrate as before in the region of the SAW period where their velocity matches that of the wave. Since now $\tilde{v}>1$, this happens at a point where the velocity gradient is negative; any carrier left behind moves forward and any carrier ahead is delayed, so that a narrow and stable charge package is formed, which subsequently translates with the SAW velocity. The package position within the SAW period is determined by the mobility and the amplitude of the field, whereas its width is determined by the diffusivity. In this case, we have a genuine SAW-induced charge transport.

The conclusion derived from the previous analysis, namely that the condition for SAW-induced transport is $\tilde{v}>1$, holds as long as diffusion effects are not significant. A large increase of the diffusivity induces a type of carrier motion independent of the velocity field, which eventually compensates the action of the wave and modifies the transport picture displayed in Fig. 3(c). One way to accomplish this regime in practice is by increasing the temperature. In order to illustrate this effect, we show in Fig. 4 the spatiotemporal dynamics of $p(x,t)$ obtained after increasing the temperature to 300 K, so that $D_p\simeq25.85$ cm^2/s and $\tilde{d}=0.155$, whereas $\tilde{v}$ is kept to the value of 1.5. Since $\tilde{v}>1$, there is indeed SAW-induced transport, with most of the carriers residing next to the nodes of the velocity field. However, the diffusivity is so large that the spatial distribution of the transported carriers widens and the carriers spill off to the lagging SAW periods. We have a situation qualitatively similar to that in Fig. 3(b), but where the SAW-induced transport is destroyed by an increase of the temperature (i.e., the diffusivity). The configuration of Fig. 4, where the carrier distribution drifts in the direction of propagation of the SAW and widens due to diffusion, resembles that of the Haynes-Shockley experiment,[27] with the difference that the spatial profile of $p(x,t)$ is modulated with the SAW wavelength.

In this section we have made a simplified analysis which is useful to understand the complete simulations of the photoluminescence dynamics to be presented later, incorporating the space-charge field, the generation-recombination terms, and the coupling with the excitons. Although the excitons are not directly transported by the SAW in the framework of our model, these particles form through the binding of free electron and holes. Therefore, the transport properties of these carriers are of paramount importance for the spatial dynamics of the exciton population and the associated emission.

B. Photoluminescence as a function of position

As shown in the preceding section, the SAW modulates the distribution of electrons and holes in space and time, and, under appropriate conditions, is able to drag the carriers with

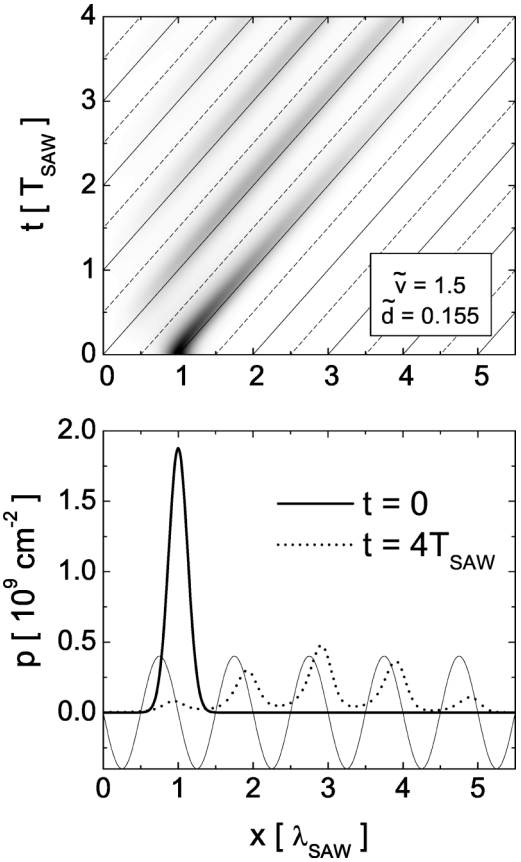

FIG. 4. Concentration $p(x,t)$ calculated from Eq. (6) as in Fig. 3(c), but for a normalized diffusivity $\tilde{d}=0.155$. The maximum concentration is $p_{\max}=1.9\times10^{9}$ cm^{-2}.

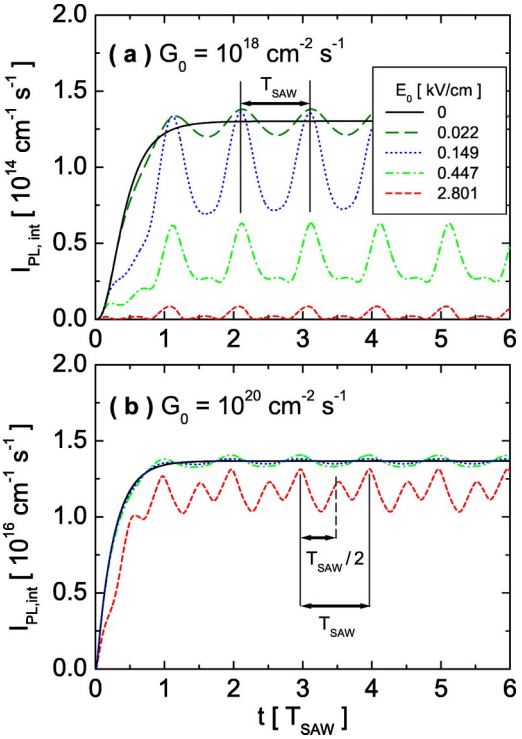

FIG. 5. (Color online) Time evolution of the PL intensity recorded at the illumination spot for two excitation conditions: (a) $G_0=10^{18}$ cm^{-2} s^{-1} and (b) $G_0=10^{20}$ cm^{-2} s^{-1}. In each case, several SAW fields are considered: $E_0=0$, 0.022 ($\tilde{v}^{(n)}=0.75$, $\tilde{v}^{(p)}=0.075$), 0.149 ($\tilde{v}^{(n)}=5$, $\tilde{v}^{(p)}=0.5$), 0.447 ($\tilde{v}^{(n)}=15$, $\tilde{v}^{(p)}=1.5$), and 2.801 kV/cm ($\tilde{v}^{(n)}=94$, $\tilde{v}^{(p)}=9.4$).

the SAW velocity. It has been experimentally demonstrated that this spatiotemporal dynamics can be easily visualized by monitoring the PL originating from the recombination of photogenerated electron-hole pairs (or the excitons formed out of them).[3,5,8–11,13,16,17] However, only few theoretical investigations have been presented so far to interpret these experiments. In this section, we present a series of systematic simulations of the effects of a traveling SAW on the PL dynamics, based on the model introduced in Sec. II. Note that, in a realistic situation, the progressive broadening of the charge packages due to diffusion in the direction perpendicular to the propagation can, in practice, hinder the SAW-induced transport. These transversal diffusion effects, which are not taken into account by our model, would surely quantitatively modify the results of the simulations reported below. In Refs. 16 and 17, it has been proposed and demonstrated that the transversal diffusion can be eliminated by transporting the carriers in a QWR oriented parallel to the SAW propagation direction. Our one-dimensional model applies directly to this situation.

In all the simulations presented below, we use the following mobilities: $\mu_n=10\,000$ and $\mu_p=1000$ cm^2/V s. These values are reasonable for a medium-quality GaAs/(Al,Ga)As QW at low temperature. We verified that the same qualitative results were obtained for carrier mobilities in a wide range around these values, as long as $\mu_n \gg \mu_p$. For the exciton diffusivity D_X, we take the value of the electron-hole ambipolar diffusivity, $D_X=2.2$ cm^2/s.[27] The other parameters are listed in Table I. Since $r \ll c$, we found the band-to-band recombination i_{PL} to be negligible as compared to the excitonic recombination I_{PL}. Therefore, we will focus only on the analysis of I_{PL}.[28] In the following, we investigate two different situations relevant to the experiments: (i) first, we will consider the case of coincident illumination and detection areas (local PL), and (ii) afterwards, we will treat the case where the PL is detected far away from the generation position along the SAW propagation direction (remote PL). In all the simulations presented hereafter, the generation spot is located at $x_s=\lambda_{\mathrm{SAW}}$ and the phase of the SAW ϕ is chosen such that at $t=0$ the spot coincides with a maximum of Φ_{SAW}, i.e., $\phi=-\frac{1}{4}$. We point out that the qualitative results discussed below are independent of the initial condition given by ϕ, which only determines the detailed shape of the PL transient.

1. Local photoluminescence

Figure 5 shows calculated time-resolved traces of the PL recorded at the same region where cw photoexcitation is applied. The emitted intensity $I_{\mathrm{PL}}(x,t)$ is integrated around the generation spot (from $x_s-\Delta_s/2$ to $x_s+\Delta_s/2$) to give a quantity $I_{\mathrm{PL,\,int}}(t)$ in units of photons/(cm s).[29] In order to study the influence of the acoustic power on $I_{\mathrm{PL,\,int}}$, we display

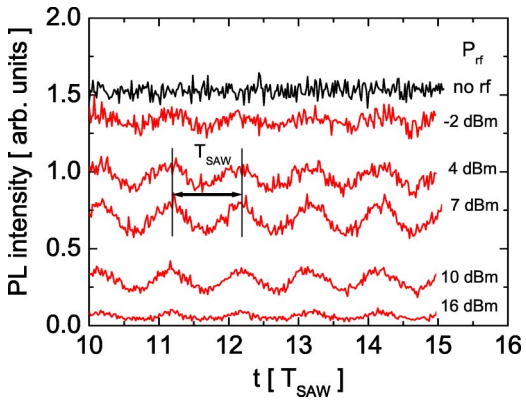

FIG. 6. (Color online) Time-resolved PL of a GaAs QW measured for coincident excitation and detection areas in the configuration of Fig. 1. The photoexcitation intensity is ~ 100 W/cm^2. The SAW intensity is specified in terms of the nominal rf power P_{rf} applied to the IDT. After correcting for coupling losses, $P_{\mathrm{rf}}=16$ dBm is estimated to yield a field amplitude of $E_0 \simeq 3$ kV/cm. The SAW frequency is 520 MHz.

results for various SAW field amplitudes E_0. An independent factor that can influence the PL spatiotemporal dynamics is the photoexcitation intensity. To illustrate its effects, we present results for two generation rates $G_0=10^{18}$ [Fig. 5(a)] and 10^{20} cm^{-2} s^{-1} [Fig. 5(b)], which roughly correspond to an external excitation intensity of 30 and 3000 W/cm^2, respectively, for an illumination spot with a diameter of 2 μm.

We shall first discuss the *low-excitation* case of Fig. 5(a). For $E_0=0$, i.e., in the absence of SAW, we observe the onset of a stationary PL trace after a transient whose characteristic time is governed, within our model, by the parameters G_0, c, and τ_X. When a SAW is applied, two interrelated effects are observed: (i) The $I_{\mathrm{PL,\,int}}$ traces are no longer stationary, but show instead a temporal modulation with the SAW period T_{SAW}, and (ii) the average PL intensity decreases as the magnitude of the SAW field increases. The last effect has been thoroughly observed in time-integrated PL experiments and usually attributed to the quenching of the PL as a consequence of the separation of the electrons and holes by the piezoelectric field accompanying the SAW.[3–7,9,16] Our detailed simulations confirm this interpretation: the photocreated electrons and holes are separated and trapped in the maxima and minima, respectively, of the moving piezoelectric potential, this process being more effective for high SAW amplitudes. The superimposed modulation has also been experimentally observed in Refs. 9, and 16. For illustrative purposes, we present in Fig. 6 a typical example of the local PL measured in a GaAs/(Al,Ga)As QW for different SAW intensities (specified in terms of the rf power P_{rf} applied to the acoustic transducers). The experimental conditions are described in detail in Ref. 11. The experiments also show a modulation with the SAW period, which initially increases with P_{rf} (for $P_{\mathrm{rf}}<7$ in Fig. 6), but then decreases for higher SAW intensities. The overall behavior is similar to that shown in the simulations of Fig. 5(a). The simulations predict that the exact shape of the modulation also depends on the power of the SAW: as the field increases, the profile evolves from a structure with a single peak in each period to the appearance of a weak secondary peak separated by $\sim T_{\mathrm{SAW}}/2$ from the main peaks. The secondary peaks expected for high acoustic powers are not resolved in the experimental results of Fig. 6, probably due to the finite time resolution and to the small signal-to-noise ratio.

In order to understand the origin of the modulation of the PL intensity, we show in Fig. 7 the spatiotemporal dynamics of excitons, electrons, and holes for the highest field displayed in Fig. 5 ($E_0=2.801$ kV/cm). For this field, the dimensionless parameters $\tilde{v}^{(n)} \equiv \mu_n E_0 / v_{\mathrm{SAW}} = 94$ and $\tilde{v}^{(p)} \equiv \mu_p E_0 / v_{\mathrm{SAW}} = 9.4$ are much larger than 1. According to the discussion in Sec. III A, the SAW in this case is very efficient in trapping the electrons and holes in the piezoelectric potential maxima and minima adjacent to the spot and transporting them with the velocity of the wave (see the plots of n and p in Fig. 7). Since the carriers are continuously generated, as the electrons stored in a potential maximum cross the excitation spot, they meet the newly generated holes spilling off to the preceding potential minimum. The increased overlap of both distributions (increased value of np) leads to the formation of excitons (see the plot of N in Fig. 7) and the subsequent PL emission. This picture accounts for the main peaks (labeled $e \rightarrow h$ in Fig. 7) in the simulated PL traces of Fig. 5. The reciprocal process, namely the increase of the PL intensity when the holes residing on a potential minimum cross the spot region, accounts for the weaker peaks (labeled $h \rightarrow e$ in Fig. 7) separated by $T_{\mathrm{SAW}}/2$ from the main peaks. The repetition of these processes gives a characteristic modulation of the PL with the periodicity of the SAW. The difference in the amplitude of both types of peaks is due to the difference in the mobilities of electrons and holes:[9] since $\mu_p \ll \mu_n$, the concentration of holes in the spot, when it is crossed by a potential maximum, is larger than that of electrons, when it is crossed by a potential minimum (see Fig. 7). Therefore, more recombination events are expected when an electron package crosses the spot. This asymmetry should be reduced for even larger fields, eventually leading to PL peaks of equal intensity for both processes, i.e., to a modulation of the PL intensity with period $T_{\mathrm{SAW}}/2$. Nevertheless, this will be accompanied by a strong reduction of the PL intensity, which can make this regime experimentally undetectable.

If, on the other hand, the SAW power is reduced [see, for example, the case of $E_0=0.447$ kV/cm in Fig. 5(a), which corresponds to $\tilde{v}^{(n)}=15$ and $\tilde{v}^{(p)}=1.5$], the holes are less efficiently transported, and there is always an appreciable quantity of them in the spot. As a consequence, the PL background increases, and the relative amplitude of $h \rightarrow e$ to $e \rightarrow h$ peaks is reduced. A further reduction of the field can lead to the situation, where the electrons are transported, but the holes not. This is the case for $E_0=0.149$ kV/cm ($\tilde{v}^{(n)}=5$ and $\tilde{v}^{(p)}=0.5$) in Fig. 5(a). Since the hole distribution is not transported but, instead, oscillates back and forth as in Fig. 3(a), the $h \rightarrow e$ peaks associated with the transit of the holes across the spot disappear. We are then left with the PL pulses due to the passage of the electrons. If we further decrease the field to the regime where neither electrons nor holes are transported, as for the case $E_0=0.022$ kV/cm ($\tilde{v}^{(n)}=0.75$ and $\tilde{v}^{(p)}=0.075$) in Fig. 5(a), the PL background

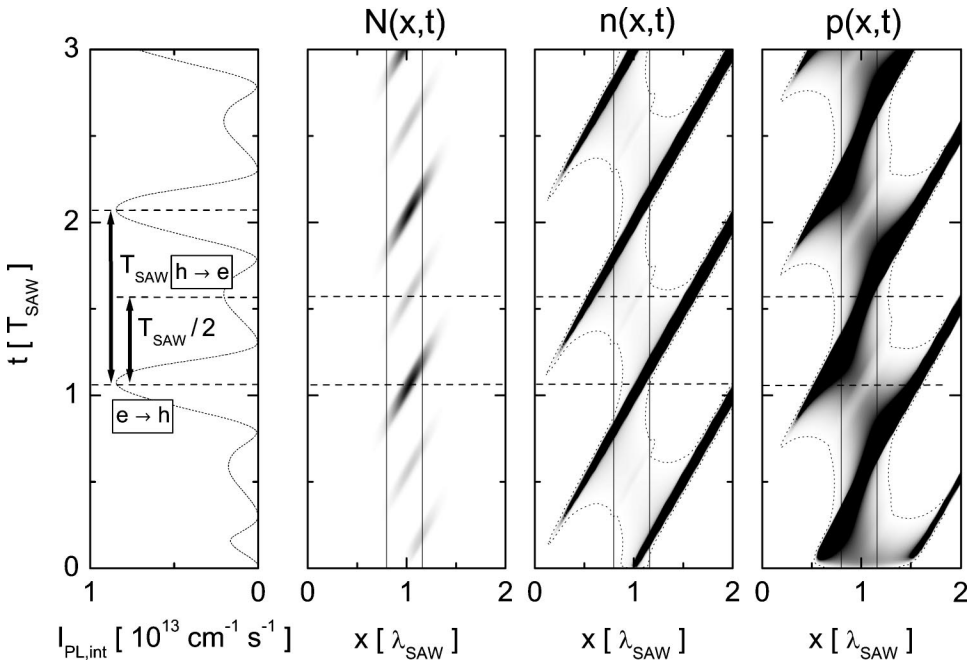

FIG. 7. The left-hand panel reproduces the time evolution of the integrated PL intensity calculated at the generation spot (situated at $x_s=\lambda_{SAW}$) for $E_0=2.801$ kV/cm [also shown in Fig. 5(a)]. The other three panels show gray scale plots in the (x,t) plane of the concentration of excitons (N), electrons (n), and holes (p). For excitons, the gray scale ranges between 0 to $N_{max}=7.3\times10^7$ cm^{-2}. For a better display, in the case of electrons and holes, the gray linear scale goes from 10^6 (dotted contour line) to 5×10^7 cm^{-2}. The concentrations below and above these values are shown as white and black areas, respectively. The vertical straight lines indicate the region where the PL intensity for the left-hand panel has been integrated.

increases and only a weak modulation remains due to the oscillations of the electron distribution in the spot region (the hole distribution remains virtually unaffected by the field).

The transport regime in which the electrons are transported, but the holes not, is a transient one, which requires some clarification. In fact, as the electrons are continuously extracted from the generation region by the SAW, the hole concentration builds up in the spot region. This spatial charge unbalance gives rise to an ever increasing attractive electrostatic field that eventually will oppose the extraction of further electrons from the generation spot and block the SAW-induced transport. This behavior is not apparent in our simulations because, for the-low generation rate considered, the time necessary for the buildup of a charge unbalance large enough to block the SAW-induced transport is much longer than the time domain used for the simulations.

We now proceed to examine the *high-excitation* case of Fig. 5(b). Here, it is apparent that the impact of the SAW on the time-resolved PL is strongly reduced as compared with the case shown in Fig. 5(a): The average PL intensity is practically unaffected, and the amplitude of the modulation is extremely weak. There are two reasons for this behavior. First, the increased photoexcitation rate results in large concentrations of electrons and holes and, by virtue of the term $c\,np$ in Eq. (4), in an efficient and continuous generation of excitons. The latter are not affected by the SAW; their recombination provides the large PL background observed in Fig. 5(b). Second, as a consequence of the large values of n and p, the induced space-charge field E_{ind} acquires an enormous importance in this excitation regime. Despite the highly nonuniform profile and nontrivial dynamics of $E_{ind}(x,t)$, our detailed simulations (not shown here) demonstrate that its main effect is a considerable screening of the SAW field, breaking to a great extent the simplified picture of the acoustically driven transport introduced in Sec. III A. Thus, for example, for $E_0=0.149$ kV/cm ($\tilde{v}^{(n)}=5$ and $\tilde{v}^{(p)}=0.5$), the attraction by the holes remaining in the spot region is sufficient to overcome the effect of the SAW field on the electrons, and only a small fraction of them is transported out of the spot in spite of $\tilde{v}^{(n)}$ being greater than 1. In addition, the electrostatic repulsion among charges of the same sign becomes stronger than the confinement effect due to the SAW field, and the carrier packages turn to be much wider than in the low-generation case. These effects also contribute to the high PL levels and to the reduction of the modulation amplitude. The SAW-induced transport can be reestablished to an appreciable amount only for sufficiently high fields. For example, the recovery of the transport manifests itself for $E_0=2.801$ kV/cm as a moderate decrease of the PL intensity, which is accompanied by the emergence of a distinguishable modulation profile containing peaks associated with the $e\rightarrow h$ and $h\rightarrow e$ processes explained above.

Finally, we briefly comment on the role of the field-induced exciton ionization in the simulations presented in Fig. 5. We have found that it only becomes important for the highest field considered, $E_0=2.801$ kV/cm, especially in the low-excitation case. In addition, the effect of the field-

induced ionization is quantitative and does not alter the main features of the time-resolved PL traces. The reason for this behavior is that, within the model adopted (see Sec. II B), and for the parameters we use, the critical field E_c for which $\tau_{\rm ion}(E_c) \simeq \tau_X$ is quite high, $E_c \sim 1.2$ kV/cm. For fields below E_c, most of the excitons recombine before they can be ionized by the SAW field. Our simulations, therefore, cast some doubt about the picture of the SAW-induced transport as a two-step process, in which the photogenerated excitons are first field ionized, and the resulting free electrons and holes are then spatially separated and transported by the wave.[6] Instead, we have shown that, when the carriers are generated above the band gap and they are sufficiently mobile, they can be separated and transported before forming bound excitons. Nevertheless, in order to decide which type of microscopic processes are present or dominant in the SAW-induced transport, more systematic experiments and more refined theoretical modeling are needed. In this respect, it seems desirable to include in further analyses other exciton dissociation mechanisms, such as the ionization by impact with the carriers accelerated by the field, whose role has been stressed in Ref. 30.

2. Remote photoluminescence

Another striking manifestation of the SAW-induced separation, storage, and transport of electrons and holes is the possibility of disposing of this long-lived excitation at a position away from the place where it was generated.[3] In order to do this, it is necessary to eliminate the agent keeping the carriers separated while moving them, namely the SAW piezoelectric potential. This is usually done by placing a metal stripe on the path of the SAW, so that its piezoelectric field is screened and, therefore, the transport is inhibited leaving the carrier dynamics governed only by diffusion effects.[3,9,10,16] In order to investigate the recombination dynamics at a remote point, we have simulated the screening of the piezoelectric potential by a metal stripe across the SAW propagation path using the simple expression:

$$\Phi_{\rm SAW}(x,t) = \frac{1}{2}\left(\tanh\frac{x-x_m}{a_m} - 1\right) \times \Phi_0 \sin\left[2\pi\left(\frac{x}{\lambda_{\rm SAW}} - \frac{t}{T_{\rm SAW}} + \phi\right)\right], \quad (7)$$

from which we obtain the SAW field as $E_{\rm SAW}(x,t) = -(\partial/\partial x)\Phi_{\rm SAW}(x,t)$. The parameters x_m and a_m give the position and half-width of the transition region between the free surface and the metal stripe. It is easy to see that the model formula (7) yields the desired behavior for the field: if $x \ll x_m$, we recover expression (2), whereas $E_{\rm SAW} \to 0$ for $x \gg x_m$. In the simulations presented below we have taken $x_m = 4\lambda_{\rm SAW}$ and $a_m \simeq 0.18\lambda_{\rm SAW}$. It is to be noted that the screening of the SAW potential is in general more complicated than the idealized form given by Eq. (7).[31]

In accordance with the discussion in Sec. III A, we have found in our simulations that, as long as $\tilde{v}^{(p)} > 1$ and $\tilde{v}^{(n)} > 1$, there is sustained ambipolar transport of electrons and holes, and, therefore, appreciable PL is observed at the remote position. In Fig. 8, we present the calculated time evolution of the PL intensity detected at the metal stripe region for the two highest values of the SAW field presented in Fig. 5: $E_0 = 0.447$ and 2.801 kV/cm. Here, $I_{\rm PL,\,int}(t)$ is the integral of $I_{\rm PL}(x,t)$ from $x_m - a_m$ to the end of the simulation domain $(5.5\lambda_{\rm SAW})$. The simulations are performed again for the two values of G_0 representative of low-excitation and high-excitation conditions listed in Sec. III B 1.

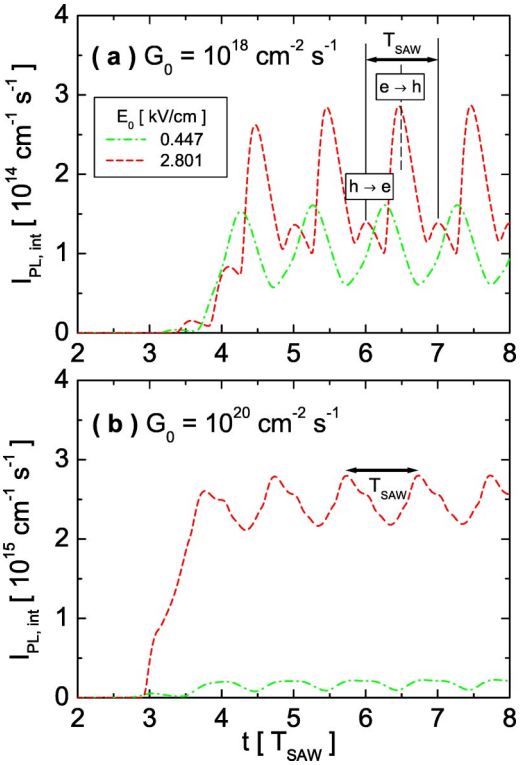

FIG. 8. (Color online) Calculated time evolution of the PL intensity underneath a metal stripe placed at a distance $x_m = 4\lambda_{\rm SAW}$ away from the generation spot. The metal stripe is used to screen the SAW potential. The calculations are shown for two excitation conditions: (a) $G_0 = 10^{18}$ cm^{-2} s^{-1} and (b) $G_0 = 10^{20}$ cm^{-2} s^{-1}. In each case, two SAW fields are considered: $E_0 = 0.447$ ($\tilde{v}^{(n)} = 15$, $\tilde{v}^{(p)} = 1.5$) and 2.801 kV/cm ($\tilde{v}^{(n)} = 94$, $\tilde{v}^{(p)} = 9.4$). The corresponding traces at the generation point are displayed in Fig. 5.

The PL traces shown in Fig. 8 also exhibit a temporal modulation with the periodicity of the SAW and are superimposed on a constant background, which is due to the finite lifetime of the excitons. The results in Fig. 8 confirm the experimental findings in Refs. 3 and 16 that the remote PL intensity follows an inverse relationship with the SAW field as compared to the local PL. The partial inhibition of the SAW-induced transport for the high-generation case already commented in Sec. III B 1 is also apparent in Fig. 8(b). Here, we see that the maximum ratio of remote to local PL intensity is only ~ 0.2, whereas it reaches ~ 100 in the low-generation case.

Regarding the exact shape of the modulation in the low-excitation regime [Fig. 8(a)], each period exhibits a double-peak structure for $E_0 = 2.801$ kV/cm. Its origin is basically the same as for the double-peak structure observed in Fig. 7: The $h \to e$ ($e \to h$) peaks correspond to the PL triggered upon

the arrival of the hole (electron) packages at the metal stripe and the subsequent recombination with residual carriers there. The difference in the amplitude of peaks $h \rightarrow e$ and $e \rightarrow h$ is again related to the fact that the electrons are more diffusive than the holes. When the latter arrive at the metal gate in a $h \rightarrow e$ process, they find a widely spread electron distribution, so that the product np (and the ensuing PL intensity) is smaller than in a $e \rightarrow h$ process, in which the incoming electrons meet a narrower distribution of holes. On the other hand, if the SAW field is low enough, as for the case $E_0 = 0.447$ kV/cm in Fig. 8(a), the modulation of the PL traces shows only a single broad peak. This behavior can be traced back to the relative position of the transported electron and hole packages within the SAW. While the electrons, given the large value of $\tilde{v}^{(n)}$ $(=15)$, travel on the SAW potential maxima, the holes, due to the moderate value of the parameter $\tilde{v}^{(p)}$ $(=1.5)$, travel somewhat delayed with respect to the minima, in a position quite close to that of the electrons. The PL from a $h \rightarrow e$ process does not have time to decay before the arrival of the electrons and the onset of the $e \rightarrow h$ process. Therefore, the $h \rightarrow e$ processes are not distinctly resolved as peaks in the PL traces, which are governed by the $e \rightarrow h$ ones. The interpretation just described also holds for the high-generation case of Fig. 8(b), but the carrier packages transported by the SAW are so wide (due to the screening by the field E_{ind}) that most of the structures in the PL traces are washed out. In the experiments performed on QW's (Ref. 9) and QWR's (Ref. 16), the PL modulation reported only exhibits single peaks separated by T_{SAW}: this can be partly explained by the difference in mobilities between electrons and holes, especially in the case of QW's, where the lateral diffusion (not taken into account in our model) can lead to the virtual disappearance of the $h \rightarrow e$ peaks.

C. Influence of potential fluctuations on the SAW-induced transport

Another interesting problem related to the SAW-induced transport of carriers and the subsequent PL is how it is affected by the presence of potential fluctuations along the SAW path. Hereafter, we shall use the term *defect* in a generalized sense as any static modulation of the potential felt by the carriers without paying attention to its physical nature. In practice, the origin of these defects can be impurities, traps, composition fluctuations, etc. Experimental evidence for recombination triggered by defects in the path of a SAW transporting electrons and holes has been given in Refs. 10 and 17. One can even consider confining potentials such as quantum wires or quantum dots as included within our definition of defects. Thus, for example, Ref. 16 has experimentally investigated the PL induced by a QWR transverse to the SAW propagation direction. Reference 32 has shown that self-assembled quantum dots can act as very efficient recombination centers for carriers transported by SAW's.

In order to quantitatively assess the influence of these defects, we introduce here a simple procedure which allows

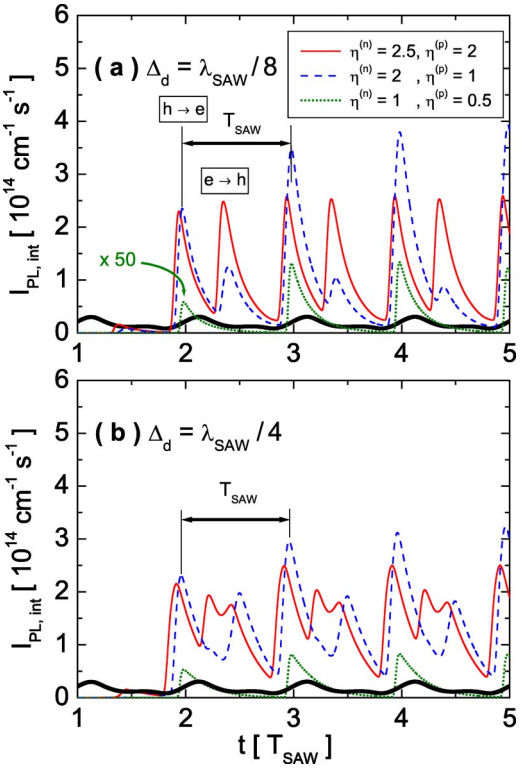

FIG. 9. (Color online) Calculated time evolution of the PL intensity at a defect for two choices of the defect size: (a) $\Delta_d = \lambda_{\text{SAW}}/8$ and (b) $\Delta_d = \lambda_{\text{SAW}}/4$. In each case, several values of the defect potential are considered: $(\eta^{(n)}=2.5,\ \eta^{(p)}=2)$, $(\eta^{(n)}=2,\ \eta^{(p)}=1)$, and $(\eta^{(n)}=1,\ \eta^{(p)}=0.5)$. The heavy solid line represents the PL intensity at the generation spot.

its investigation in the framework of our model. First, we propose the following simple form for the potential induced by the defect:

$$\Phi_d(x) = U_d\left(\tanh^2\frac{x-x_d}{a_d} - 1\right), \tag{8}$$

where x_d and a_d give the position and lateral dimensions of the defect (the full width at half maximum of the potential is $\Delta_d = 2\,a_d \cosh^{-1}\sqrt{2} \simeq 1.76\,a_d$). The depth of the defect potential is given by $|U_d|$ whereas the sign of U_d determines if it is a well-type or barrier-type defect. The potential in Eq. (8) is then incorporated into the transport equations by adding the associated electric field $E_d(x) = -(\partial/\partial x)\Phi_d(x)$ to the electric field $E = E_{\text{SAW}} + E_{\text{ind}}$, and thereafter the simulations are performed in the usual way. With this model, we can simulate any combination of defects, including those which act only on one or on both types of carriers. For definiteness, we will investigate the situation, in which there is a defect of extension Δ_d at $x_d = 2.5\lambda_{\text{SAW}}$, which acts as a well for electrons and holes, i.e., $U_d^{(n)} < 0$ and $U_d^{(p)} > 0$. This choice of potential will illustrate the trapping dynamics of electrons and holes, and, moreover, will simulate the specific situation found in Ref. 16, where the SAW is launched transversally to a QWR embedded in the QW.

The relevant parameter controlling the interplay between the defect and the SAW-induced transport is the ratio η

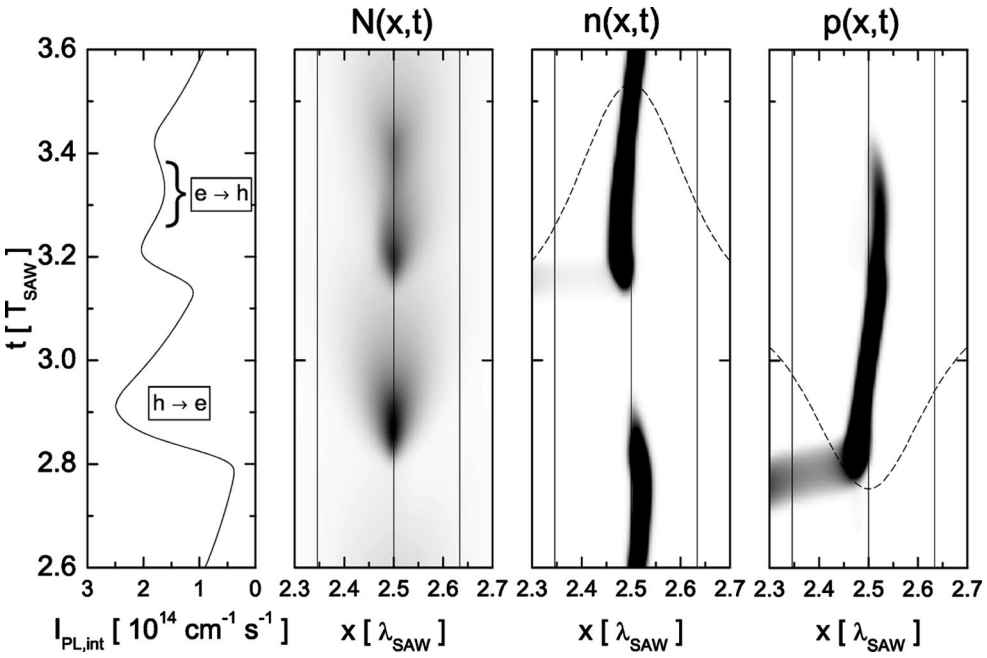

FIG. 10. The left-hand panel reproduces the time evolution of the PL intensity recorded at the defect for $\eta^{(n)}=2.5$ and $\eta^{(p)}=2$, as already shown in Fig. 9(b). The other three panels show gray scale plots in the (x,t) plane for the concentration of excitons (N), electrons (n), and holes (p). For excitons the gray scale ranges from 0 to $N_{\max}=2.9\times10^9$ cm^{-2}, whereas for electrons and holes it goes from 0 to 3×10^9 cm^{-2}. The concentrations above this value are shown as black areas. The superimposed dashed curves show the profile of the defect potential for electrons and holes. The vertical straight lines indicate the center and limits of the region where the PL intensity for the left-hand panel has been integrated.

$=E_{d,\max}/E_0$, where $E_{d,\max}$ is the maximum value of the field $E_d(x)$ [for the potential given in Eq. (8), $E_{d,\max}=(4\sqrt{3}/9)\times(|U_d|/a_d)\simeq0.77(|U_d|/a_d)$]. As a rule of thumb, the carriers can be indefinitely trapped by the defect potential only if $\eta>1$. Otherwise, the carriers are temporarily trapped until the arrival of a field maximum, which overcomes the defect potential and releases the carriers for subsequent transport by the wave.

In Fig. 9, we present simulations of the defect-induced recombination for two cases: $\Delta_d=\lambda_{\mathrm{SAW}}/8$ (hereafter referred to as *small defect*) and $\Delta_d=\lambda_{\mathrm{SAW}}/4$ (*large defect*). For each case, we have adjusted the defect potential depths for electrons $(U_d^{(n)})$ and holes $(U_d^{(p)})$ in order to explore the range of values for $\eta^{(n)}$ and $\eta^{(p)}$ around 1. The SAW field is taken to be $E_0=1.120$ kV/cm ($\tilde{v}^{(n)}=38$, $\tilde{v}^{(p)}=3.8$) so that both the electrons and holes can be efficiently transported in the QW. The generation rate $G_0=10^{18}$ cm^{-2}s^{-1}, which corresponds to the low-excitation conditions considered before, is used in the calculations. $I_{\mathrm{PL,\,int}}(t)$ is defined here as the integral of $I_{\mathrm{PL}}(x,t)$ from $x_d-\Delta_d/2$ to $x_d+\Delta_d/2$.

Let us first focus on the small-defect case in Fig. 9(a). For the largest defect potential ($\eta^{(n)}=2.5$, $\eta^{(p)}=2$), two families of peaks are again observed, each of them with the periodicity of the SAW. Their origin is the same as for the double-peak structure observed in Fig. 8(a): The sequence of peaks labeled $h\rightarrow e$ $(e\rightarrow h)$ is due to the recombination that takes place when a package of holes (electrons) reaches the defect, which is already populated by trapped electrons (holes). We point out that, contrary to the situation discussed in Sec. III B, in this case the PL intensity is the same for the $h\rightarrow e$ and $e\rightarrow h$ processes. As a consequence of the strongly reduced diffusion of the trapped carriers, the difference in the mobilities of electrons and holes has a smaller impact here. When the defect potential is reduced to the case ($\eta^{(n)}=2$, $\eta^{(p)}=1$), the relative intensity of the $e\rightarrow h$ peaks diminishes, since part of the holes are now able to escape from the defect and fewer remain available for the $e\rightarrow h$ recombination processes. If the defect potential is further reduced to ($\eta^{(n)}=1$, $\eta^{(p)}=0.5$), the holes are no longer captured and the $e\rightarrow h$ peaks disappear.

In the case of large defects [Fig. 9(b)], the recombination dynamics follows essentially the same pattern as exposed above. The main difference is the appearance of an additional structure in the $e\rightarrow h$ peaks, for the largest defect potential considered ($\eta^{(n)}=2.5$, $\eta^{(p)}=2$). In order to address the physical origin of these peaks, we show in Fig. 10 the spatiotemporal dynamics of excitons, electrons, and holes for this case. The additional structure observed during the $e\rightarrow h$ process is due to the fact that the large size of the defect allows the trapped carriers to oscillate inside it as the wave passes, giving two peaks as the electrons meet twice the holes. As we reduce the defect potential to the case ($\eta^{(n)}=2$, $\eta^{(p)}=1$), the two-peak structure $e\rightarrow h$ collapses to a single one which, moreover, is smaller than the $h\rightarrow e$ peak. As in Fig. 9(a), only the $h\rightarrow e$ peaks remain for the smaller defect potentials ($\eta^{(n)}=1$, $\eta^{(p)}=0.5$). Their intensity, however, is considerably higher since now the large defect is able to retain an important fraction of the electrons. This result evidences that not only the defect potential depth but also its lateral extension plays an important role in the recombination dynamics.

IV. SUMMARY

We have presented a theoretical model for the spatiotemporal dynamics of electrons, holes, and excitons in QW's under the piezoelectric field associated with a SAW. The model has been exemplified by performing simulations in situations relevant to experiments.

In a first step, we have examined the various possible transport regimes for a single type of carrier (unipolar transport) in the framework of a simplified version of the model and found that long-distance acoustically induced transport of well-defined charge packages can be achieved provided that (i) the maximum carrier velocity μE_0 is appreciably greater than the SAW velocity and (ii) diffusion effects are not significant. Otherwise, the transport is only temporary or even absent.

We have shown that in a system containing electrons and holes with very different mobilities, it is in principle possible, by continuously increasing the SAW amplitude, to scan across the following transport regimes: (a) the *no-transport* situation, in which the SAW field is unable to drag neither electrons nor holes, (b) a *transient unipolar transport* regime, in which an initial transport of electrons is blocked in the long term by the attraction of the nontransported holes, and (c) the *sustained ambipolar transport* regime, in which both electrons and holes are transported as separate charge packages stored in the maxima and minima of the SAW piezoelectric potential, respectively. It is clear that the less mobile carriers (in our case, the holes) determine the transport regime. The different regimes lead to distinct spatiotemporal behaviors of the PL intensity, which can be accessed by time and spatially resolved PL measurements. We have shown that, as a consequence of the SAW-induced transport, the average (time-integrated) value of the PL intensity recorded at the excitation spot decreases with the SAW amplitude, while it increases at a remote position, where the piezoelectric potential is screened, in agreement with the experimental findings.[3,16] In addition, the PL intensity is found to be time modulated with the periodicity of the SAW and to exhibit one or two peaks per SAW period depending on the SAW amplitude.

Finally, the influence of extended potential inhomogeneities along the SAW path on the PL intensity has also been studied. The simulations show that, provided they are sufficiently strong, the fluctuations are able to periodically trap the transported electrons and/or holes and trigger their recombination. The PL intensity is again time modulated with the periodicity of the SAW and exhibits a fine structure, which depends on the spatial extension and depth of the potential fluctuations.

ACKNOWLEDGMENTS

We thank H. T. Grahn for comments and for a careful reading of the manuscript. This work was partially supported by the Spanish Ministerio de Ciencia y Tecnología, under the Program of Acciones Integradas (Grant No. HA2001-0043), and by the DAAD/Germany.

*Corresponding author. Electronic address: garcial@uv.es

[1] For a textbook discussion, see M. Lundstrom, *Fundamentals of Carrier Transport* (Cambridge University Press, Cambridge, 2000).

[2] D.A.B. Miller, D.S. Chemla, and S. Schmitt-Rink, in *Optical Nonlinearities and Instabilities in Semiconductors*, edited by H. Haug (Academic Press, New York, 1988), p. 325.

[3] C. Rocke, S. Zimmermann, A. Wixforth, J.P. Kotthaus, G. Böhm, and G. Weimann, Phys. Rev. Lett. **78**, 4099 (1997).

[4] K.S. Zhuravlev, D.V. Petrov, Yu.B. Bolkhovityanov, and N.S. Rudaja, Appl. Phys. Lett. **70**, 3389 (1997).

[5] P.V. Santos, M. Ramsteiner, and F. Jungnickel, Appl. Phys. Lett. **72**, 2099 (1998).

[6] C. Rocke, A.O. Govorov, A. Wixforth, G. Böhm, and G. Weimann, Phys. Rev. B **57**, R6850 (1998).

[7] O.A. Korotchenkov, A. Yamamoto, T. Goto, M.-W. Cho, and T. Yao, Appl. Phys. Lett. **74**, 3179 (1999).

[8] P.V. Santos, M. Ramsteiner, F. Jungnickel, and R. Hey, Phys. Status Solidi A **173**, 269 (1999).

[9] F. Alsina, P.V. Santos, R. Hey, A. García-Cristóbal, and A. Cantarero, Phys. Rev. B **64**, 041304 (2001).

[10] S.K. Zhang, P.V. Santos, and R. Hey, Appl. Phys. Lett. **80**, 2320 (2002).

[11] P.V. Santos, F. Alsina, S.K. Zhang, R. Hey, A. García-Cristóbal, and A. Cantarero, Physica E (Amsterdam) **13**, 467 (2002).

[12] O.A. Korotchenkov, T. Goto, H.G. Grimmeiss, C. Rocke, and A. Wixforth, Rep. Prog. Phys. **65**, 73 (2002).

[13] T. Sogawa, P.V. Santos, S.K. Zhang, S. Eshlaghi, A.D. Wieck, and K.H. Ploog, Phys. Rev. Lett. **87**, 276601 (2001).

[14] M. Rotter, A.V. Kalameitsev, A.O. Govorov, W. Ruile, and A. Wixforth, Phys. Rev. Lett. **82**, 2171 (1999).

[15] A.V. Kalameitsev, A.O. Govorov, H.-J. Kutschera, and A. Wixforth, Pis'ma Zh. Eksp. Teor. Fiz. **72**, 273 (2000) [JETP Lett. **72**, 190 (2000).

[16] F. Alsina, P.V. Santos, H.P. Schönherr, W. Seidel, K.H. Ploog, and R. Nötzel, Phys. Rev. B **66**, 165330 (2002).

[17] F. Alsina, P.V. Santos, H.P. Schönherr, R. Nötzel, and K.H. Ploog, Phys. Rev. B **67**, 161305 (2003).

[18] F. Alsina, J.A.H. Stotz, R. Hey, and P.V. Santos, Solid State Commun. **129**, 453 (2004).

[19] T. Sogawa, P.V. Santos, S.K. Zhang, S. Eshlaghi, A.D. Wieck, and K.H. Ploog, Phys. Rev. B **63**, 121307 (2001).

[20] B.K. Ridley, Phys. Rev. B **41**, 12 190 (1990).

[21] S. Selberherr, *Analysis and Simulation of Semiconductor Devices* (Springer, Vienna, 1984).

[22] The influence of the transverse component of the SAW piezoelectric field on the transport properties will be neglected due to the strong restriction to the tranverse motion imposed by the quantum well confinement.

[23] C. Piermarocchi, F. Tassone, V. Savona, A. Quattropani, and P. Schwendimann, Phys. Rev. B **55**, 1333 (1997).

[24] D.A.B. Miller, D.S. Chemla, T.C. Damen, A.C. Gossard, W. Wiegmann, T.H. Wood, and C.A. Burrus, Phys. Rev. B **32**, 1043 (1985); K. Tanaka, M. Kobashi, T. Shichiri, T. Yamabe, D.M. Silver, and H.J. Silverstone, *ibid.* **35**, 2513 (1987).

[25] T. Nakamura, R. Tanaka, T. Yabe, and K. Takizawa, J. Comput.

Phys. **174**, 171 (2001); **175**, 792 (2002).
[26] M. Grundmann and D. Bimberg, Phys. Rev. B **38**, 13 486 (1988).
[27] S.M. Sze, *Physics of Semiconductor Devices* (Wiley, New York, 1981).
[28] The product np has been taken in previous works as a measure of the excitonic recombination rate (see, for example, Refs. 9 and 15). As shown in Sec. II, this approach is not strictly correct. Nevertheless, this does not mean that the product np is completely irrelevant, since cnp gives the rate of generation of excitons at a given point, which subsequently decay radiatively. The exciton lifetime, however, may also be limited by the field-induced ionization.
[29] The results shown in Fig. 5 are, to a certain extent, dependent on the interval chosen to integrate $I_{\mathrm{PL}}(x,t)$. In order to simulate as closely as possible the experimental situation, (Refs. 9, 10, and 16) we have chosen to integrate in a symmetric interval around the spot position. Nevertheless, due to the asymmetry imposed on the system by the traveling SAW, part of the recombination takes place outside the spot and is, therefore, not taken into account in Fig. 5.
[30] S.K. Zhang, P.V. Santos, and R. Hey, Appl. Phys. Lett. **78**, 1559 (2001).
[31] G.R. Aizin, G. Gumbs, and M. Pepper, Phys. Rev. B **58**, 10 589 (1998).
[32] C. Bödefeld, A. Wixforth, J. Toivonen, M. Sopanen, and H. Lipsanen, Phys. Status Solidi B **224**, 703 (2001).